Graphene levitation and orientation control using a magnetic field

Chao Niu,[1] Feng Lin,[2,3] Zhiming M. Wang,[3,4] Jiming Bao,[2,3,5] and Jonathan Hu[1,a)]
[1]*Department of Electrical and Computer Engineering, Baylor University, Waco, Texas 76798, USA*
[2]*Department of Electrical and Computer Engineering, University of Houston, Houston, Texas 77204, USA*
[3]*Institute of Fundamental and Frontier Sciences, University of Electronic Science and Technology of China, Chengdu, Sichuan 610054, China*
[4]*State Key Laboratory of Electronic Thin Films and Integrated Devices, University of Electronic Science and Technology of China, Chengdu, Sichuan 610054, China*
[5]*Materials Science and Engineering, University of Houston, Houston, Texas 77204, USA*

(Received 18 September 2017; accepted 26 December 2017; published online 23 January 2018)

This paper studies graphene levitation and orientation control using a magnetic field. The torques in all three spatial directions induced by diamagnetic forces are used to predict stable conditions for different shapes of millimeter-sized graphite plates. We find that graphite plates, in regular polygon shapes with an even number of sides, will be levitated in a stable manner above four interleaved permanent magnets. In addition, the orientation of micrometer-sized graphene flakes near a permanent magnet is studied in both air and liquid environments. Using these analyses, we are able to simulate optical transmission and reflection on a writing board and thereby reveal potential applications using this technology for display screens. Understanding the control of graphene flake orientation will lead to the discovery of future applications using graphene flakes. *Published by AIP Publishing.* https://doi.org/10.1063/1.5005539

I. INTRODUCTION

Graphene has drawn intense interest since its discovery in 2004 due to its two-dimensional honey-comb lattice structure and unique electrical, optical, mechanical, chemical, and biocompatible properties.[1–6] Examples of graphene based devices include optical modulators,[7–10] plasmonic switches,[11,12] and biosensors.[13–15] Recent research indicates the important role of graphene flake orientation in controlling the properties of graphene flakes. When graphene flakes are assembled in the same planar direction, they exhibit unique thermal, optical, and electrical properties,[16–21] which lead to applications in thermal and electromagnetic interface materials.[16–18] These unique properties of individual nanostructures can be exploited for large-scale macroscopic functions when they are arranged in a specific macroscopic order.[22]

Diamagnetic materials, such as graphene, create a magnetic field in a direction opposite to the externally applied magnetic field, leading to a repulsive magnetic force.[23–26] Orientation control and levitation of graphene flakes are feasible with a weak magnetic field due to their high volume magnetic susceptibilities.[22,27–29] Previous research on magnetic levitation and orientation control of graphene has led to diverse applications.[28–31] It has been proposed that diamagnetism can be used to align graphene flakes.[23] A novel diamagnetic lateral force calibrator can be developed using diamagnetic levitation of graphite.[30] Optical motion control of graphite has also been demonstrated.[31] The diamagnetic properties of graphene are expected to yield numerous diverse future applications such as magnetomechanics and magnetic micro-electro-mechanical-systems (MEMS).[32–36] On the other hand, the levitation using diamagnetic materials has also been theoretically studied.[37–40] Previous theoretical studies on graphene or graphite focus on the case with diamagnetic force in one direction or the case with diamagnetic force in a uniform magnetic field.[28,39] The detailed theoretical study on the orientation control of graphene flakes has not been fully reported or used to understand physical devices. The understanding of the graphene levitation and orientation control requires studies on torques in all three spatial directions in a non-uniform magnetic field. All the recent advances in controlling graphene flakes lead to a research direction to unveil the relation between the magnetic force and the graphene flake orientation. In this paper, we study torques in all three spatial directions induced by diamagnetic forces and show the orientation control of graphene flakes using forces due to diamagnetism. First, we conduct theoretical analysis of the forces on graphite plates. Second, we examine the stable levitation condition for different shapes of graphite plates above a four interleaved permanent magnet system. Third, we analyze the tilted angle of graphene flakes above one permanent magnet. Finally, we demonstrate an ability to model the orientation of graphene flakes for the application of a display screen.

II. EXPERIMENT

Figure 1(a) shows the levitation experiment. The millimeter-sized square graphite thin plate was levitated by four permanent magnets, and a stable levitation condition existed when the graphite edge was 45° with respect to the magnet edge. Figure 1(b) shows a tilted graphite plate on a supporting board above a magnet in air. When the distance between the graphite plate and magnet changes, the tilted angle changes. Figure 1(c) shows a micrometer-sized graphene flake above a magnet in liquid. The orientation of the graphene flake changed after the magnetic field was applied. The time in Fig. 1(c) marks the elapse of time after the magnetic field was applied. One can see that the graphene flake changed orientation on the scale of seconds in response to an external magnetic field.

a)Electronic mail: jonathan_hu@baylor.edu

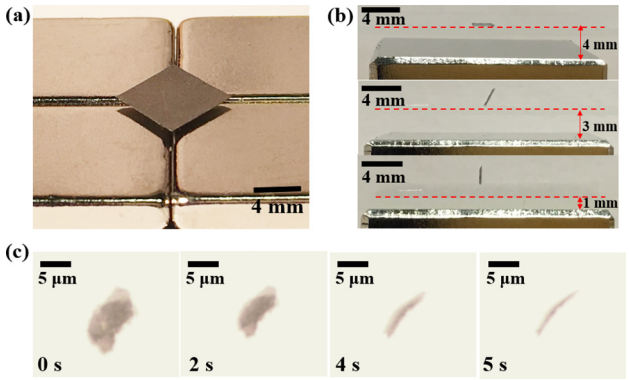

FIG. 1. (a) Graphite plate levitated by four magnets. (b) Graphite plate on a supporting board above one magnet in air. Distance between the graphite plate and magnet is marked on the figure. (c) A graphene flake after a magnetic field was applied. The elapse of time after a magnetic field was applied is marked on the figure.

III. LEVITATION USING FOUR MAGNETS

We show simulations in this section corresponding to the experiments as shown in Fig. 1. The current model and the charge model are commonly used to simulate magnetic fields.[41] The current model is often used to find magnetic fields near solenoids or cylindrical magnets.[42,43] The charge model has been used to simulate magnetic fields near rectangular magnets.[44,45] A good agreement between simulation results using the charge model and experimental results has been achieved.[46] We calculate the magnetic field using the charge model, where a magnet is modeled by a distribution of magnetic charges, and charge distribution is used to obtain the total magnetic field.[41] We use a volume magnetization of 8×10^5 A/m in our simulation, so that the magnetic field is close to the experimental data of 0.3 T near the magnet.[22] Figures 2(a)–2(c) show the magnetic fields at 0.5 mm above the top surface of four interleaved magnets. The size of each magnet is 5 mm × 5 mm × 5 mm. In Figs. 2(d)–2(f), we plot the force distribution assuming infinitely small graphite particles. We use infinitely small particles so that we can visually observe the force distribution on every position. The magnetic force is $\mathbf{F} = \int_V \mathbf{f} dV$. The force density $\mathbf{f}$ can be expressed as[28,47]

$$\mathbf{f} = (\mathbf{M} \cdot \nabla)\mathbf{B} = \frac{1}{2\mu_0} \nabla(\chi_x B_x^2 + \chi_y B_y^2 + \chi_z B_z^2), \quad (1)$$

where $\mathbf{M}$ is the effective induced magnetization, $\mathbf{B}$ is the magnetic flux density, μ_0 is the vacuum permeability, χ_x and χ_y are equal to transverse magnetic susceptibility $\chi_\parallel = -0.85 \times 10^{-4}$,[26,28] and χ_z is equal to perpendicular magnetic susceptibility $\chi_\perp = -4.5 \times 10^{-4}$.[26,28] The effective induced magnetization with the magnetic susceptibility tensor $\boldsymbol{\chi}$ in the presence of a static magnetic flux density $\mathbf{B}$ can be expressed as[28,48]

$$\mathbf{M} = \frac{1}{\mu_0} \boldsymbol{\chi} \cdot \mathbf{B}. \quad (2)$$

From Fig. 2, we try to determine the stable condition for a square graphite plate with a size of 2 mm × 2 mm × 0.2 mm at different rotational angles φ with respect to the four interleaved magnets, as shown in Fig. 3(a). The torque for a graphite plate in a magnetic field is[49,50]

$$\boldsymbol{\tau} = \int_V \mathbf{M} \times \mathbf{B} dV + \int_V \mathbf{r} \times \mathbf{f} dV, \quad (3)$$

where $\mathbf{r}$ is the position vector and $\mathbf{f}$ is the force density from Eq. (1). For a square graphite plate as shown in Fig. 3(a), the first term in Eq. (3) is zero due to the symmetry of the magnetic field, so we only need to consider the second term in order to find the stable condition. Figures 3(b) and 3(c) show the force distribution of F_x and F_y, respectively, on a square graphite plate with different rotational angles φ, defined in Fig. 3(a). The corresponding rotational direction due to F_x and F_y is also marked on the figure. We can see that the forces on graphite plates reach equilibrium when φ is 0° or 45°. However, the condition with $\varphi = 45°$ shows stable levitation even with a small rotational perturbation as shown in Fig. 3, while $\varphi = 0°$ does not show stable levitation. We show Figs. 2 and 3 in arbitrary units to illustrate the force

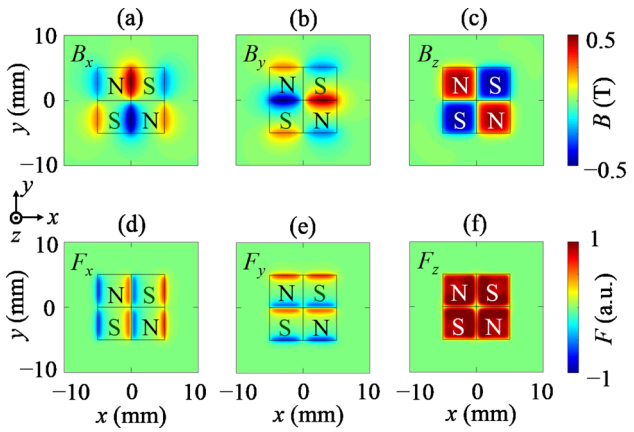

FIG. 2. Magnetic field distribution of (a) B_x, (b) B_y, and (c) B_z at 0.5 mm above the top surface of four interleaved magnets. Force distribution of (d) F_x, (e) F_y, and (f) F_z at 0.5 mm above the top surface of four interleaved magnets. The parity is also marked above the four interleaved magnets.

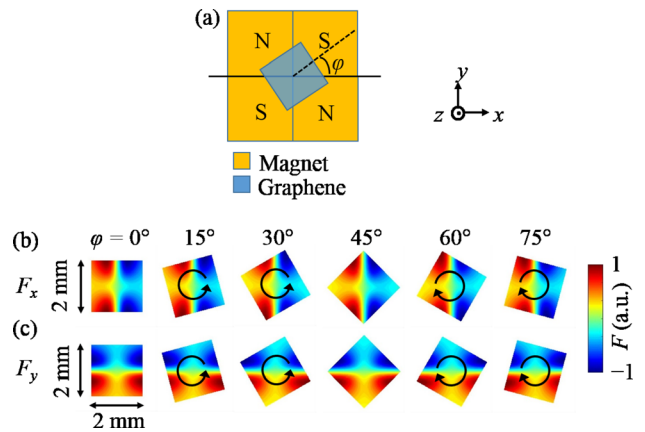

FIG. 3. (a) Schematic illustration of a square graphite plate above the four interleaved magnets. Force distribution of (b) F_x and (c) F_y for a square graphite plate with different relative angles, φ, with respect to the magnet edge. The arrows indicate the rotation direction induced by F_x or F_y.

distribution. The exact values of the force depend on the volume in the equation $\mathbf{F} = \int_V \mathbf{f} dV$. Figures S1 and S2 in the supplementary material show the exact values of the force.

Figure 4(b) shows the torques for a square graphite plate as a function of rotational angle according to Eq. (3). Note that the torque in the x-direction, $\tau_x = \int_V (y \times f_z - z \times f_y) dV$ is always zero if the graphite plate satisfies a two-fold rotational symmetry according to the force distribution shown in Fig. 2. For the same reason, $\tau_y = \int_V (z \times f_x - x \times f_z) dV$ is always zero if the graphite plate satisfies the two-fold rotational symmetry. When $\varphi = 0°$ or 45°, τ_z reaches zero, which yields an equilibrium state according to Fig. 4(b). When $\varphi = 45°$, a small perturbation towards positive rotation will induce a negative torque, which will rotate the graphite plate back towards the initial position. Hence, the graphite plate at $\varphi = 45°$ with a negative slope in the torque curve corresponds to a stable levitation position. On the other hand, when $\varphi = 0°$, a small rotational perturbation will rotate the graphite plate away from the initial position. This conclusion is in agreement with the analysis shown in Fig. 3.

We also perform a similar analysis for a graphite plate with a hexagon shape as shown in Fig. 4(d). Since a hexagon has a six-fold rotational symmetry, it automatically satisfies the two-fold rotational symmetry, thus both τ_x and τ_y are still zero. The value τ_z is zero at $\varphi = m \times 15°$, where m is an integer. The stable positions for a graphite plate with a hexagon shape are $\varphi = m \times 30°$ with a negative slope as shown in Fig. 4(d). We further study graphite plates with triangle or pentagon shapes, as shown in Fig. 4(a) or 4(c). The curves for τ_x and τ_y are not always zero for all angles φ because a triangle or pentagon does not have a two-fold rotational symmetry. The curves for τ_x, τ_y, and τ_z never become zero at the same angle. Hence, a graphite plate with a triangle or pentagon shape will never achieve a stable levitation condition and will fail to float horizontally above four interleaved magnets. Note that we only need to consider the second term on the right hand side of Eq. (3) for the square and hexagon plates due to the two-fold rotational symmetry. However, both the first term and second term in Eq. (3) have to be included for triangle or pentagon plates. Our analysis can be extended to additional polygons. In order to achieve a stable horizontal levitation condition, graphite plates in regular polygon shapes require a two-fold rotational symmetry with an even number of sides. In contrast, a graphite plate in a regular polygon shape with an odd number of sides only has an odd number fold rotational symmetry and will never reach a stable horizontal levitation condition. Of course, a graphite disk with a rounded shape, which is equivalent to a regular polygon with an infinite number of sides, satisfies the two-fold rotational symmetry and yields a stable levitation condition.[31] In the above analysis, we maintain a constant graphite plate area of 4 mm^2 and a thickness of 0.2 mm.

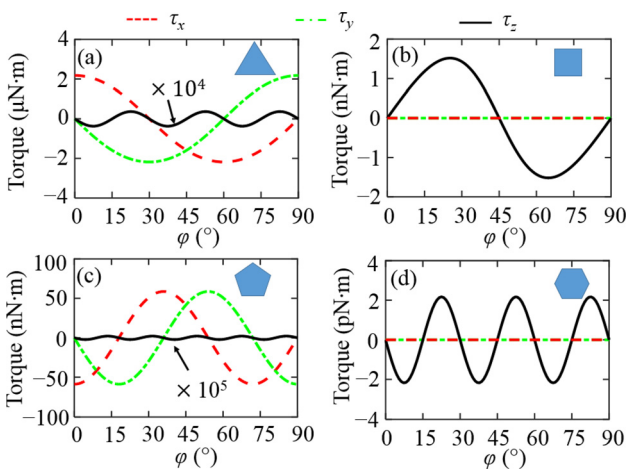

FIG. 4. Torques as a function of rotational angle with graphite shapes of equilateral (a) triangle, (b) square, (c) pentagon, and (d) hexagon. τ_z is multiplied by 10^4 in (a) and by 10^5 in (c). The insets show the shapes of different regular polygons.

In addition, we study potential energy to confirm previous analysis on the stable condition using torque. The total potential energy for the graphite plate is calculated using the following equation:[28,41]

$$U = -\int_V \mathbf{M} \cdot \mathbf{B} dV, \tag{4}$$

where $\mathbf{M}$ is the effective induced magnetization and $\mathbf{B}$ is the magnetic flux density at the location of the particle. The position with the lowest potential energy due to diamagnetism could indicate a stable condition. Figures 5(a) and 5(b) show the total potential energy for square and hexagon graphite plates as a function of relative angle φ, which is defined in Fig. 3(a). The angles with the lowest potential energy corresponding to the stable condition, as shown in Fig. 5, are consistent with the study using torque, as shown in Fig. 4.

Previous paragraphs study the rotation of graphite plates due to the diamagnetic force. We now study the levitation height due to the diamagnetic force on four interleaved magnets. Figure 6(a) shows the levitation height for a square plate as a function of the side length of the plate when the thickness of graphite plate is fixed at 0.2 mm. The levitation height is the distance between the magnets and the graphite plate when the levitation force and the gravity force are balanced. The density of graphite is 2.22×10^3 kg/m^3.[37] When the graphite side length is shorter than twice the side length of magnets, the increase of the graphite surface area will increase the levitation force according to Fig. 2(f). When the graphite side length is much longer than twice the side length of magnets, the increase of the graphite surface area does not significantly increase the levitation force. In this case, increasing the graphite plate side length primarily increases the weight of the graphite plate, and the levitation height decreases as the side length of the graphite plate increases.

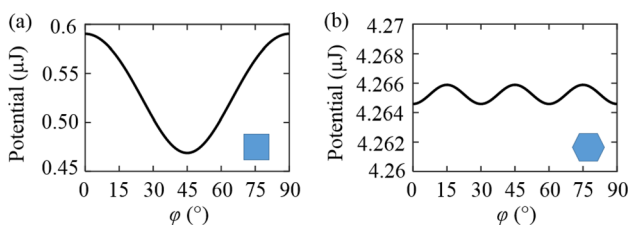

FIG. 5. Potential energy as a function of rotational angle for a graphite plate in (a) a square shape or (b) a regular hexagon shape. The insets show the shapes of graphite plates.

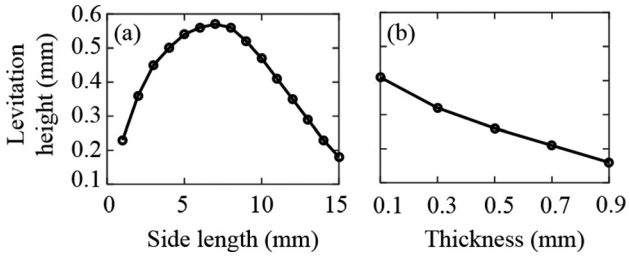

FIG. 6. (a) The levitation height as a function of side length of a graphite plate when the graphite thickness is fixed at 0.2 mm. (b) The levitation height as a function of thickness of the graphite plate when the graphite side length is fixed at 2 mm.

Figure 6(b) shows that the levitation height also decreases when the thickness of the graphite plate increases due to the increase in weight of the graphite plate. Because the magnetic force decreases exponentially along the z-axis, the levitation height decreases as the thickness and weight of a graphite plate increase. The levitation force and the gravity force as a function of distance between the magnets and the graphite plate are shown in Fig. S3 (supplementary material). We wrote our own code to find magnetic fields, magnetic forces, and torques. We obtained a good agreement between the magnetic fields calculated using our own code and commercial software COMSOL.

IV. ORIENTATION CONTROL USING ONE MAGNET

Figures 1(b) and 1(c) show a millimeter-sized graphite plate and a micrometer-sized graphene flake in air and liquid, respectively. There is no fundamental difference in the studies of the forces due to diamagnetism between micrometer-sized graphene flakes and millimeter-sized graphite plates. One magnet can control the orientation of the graphene flakes as four magnets are needed for a stable levitation experiment. Due to diamagnetism, the graphene flake is tilted with a magnetic field. The control of nano- or micro-particles using a magnetic field has several beneficial features, such as contactless, non-invasive, and biocompatible.[28] We now study the direction of a small graphene flake when it is placed above one magnet, as shown in Fig. 1(b). The individual magnet has a size of 5 mm × 5 mm × 5 mm and the micrometer-sized graphene flake has a size of 10 μm × 10 μm × 5 nm. In the presence of a magnetic field, the particle experiences torques due to the magnetic field represented by Eq. (3). Our numerical simulations show that the first term on the right hand side of Eq. (3) always dominates in the study in this section.

Figure 7(a) shows the schematic of a graphene flake with a tilted angle θ in air on top of a thin supporting board. We assume a relative permeability of 1.0 for the supporting board, which does not change the magnetic field. The tilted angle θ is found when the torque due to the magnetic field from Eq. (3) equals the torque induced from gravity. In Fig. 8, we plot τ_G as the torque due to the gravity and τ_m as the torque due to the magnetic field at different values of z and x. We use τ_m in a direction which is opposite to the direction of τ_G so the balanced position occurs when $\tau_G = \tau_m$. When $z = 4$ mm and $x = 0$ mm, there are two intersect points between the curves of τ_m and τ_G, as shown in

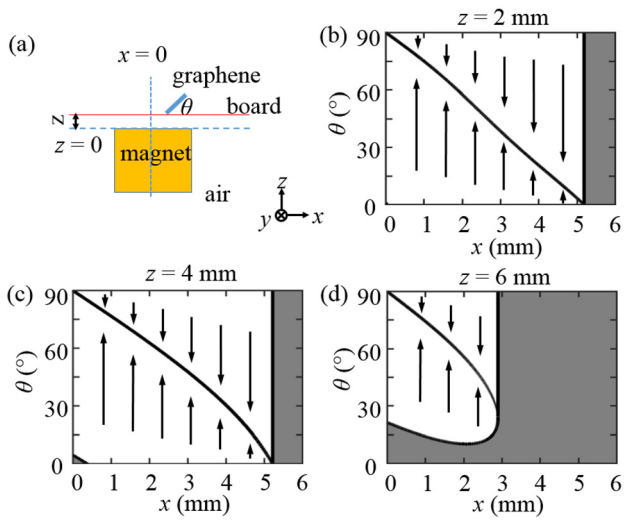

FIG. 7. (a) Schematic illustration of a graphene flake in air. Initial and final tilted angles when the graphene flake moves along the x-direction in air at (b) $z = 2$ mm, (c) $z = 4$ mm, and (d) $z = 6$ mm. Gray region: the final angle is 0. White region: the final angle is on the solid curve with the same x distance according to the direction indicated by the black arrows.

Fig. 8(a). We note that τ_m is less than τ_G and the graphene flake will fall down when the initial tilted angle is less than the first intersect point at $\theta = 5°$. Otherwise, the flake will stand up and rotate to the angle corresponding to the second intersect point at $\theta = 90°$. As one moves the flake away from the magnet at $x = 2$ mm, there is only one intersect point between the curves of τ_m and τ_G as indicated by Fig. 8(b). The final tilted angle will end up with one unique solution of $\theta = 63°$ no matter what the initial titled angle is. If the graphene flake moves further away from the magnet at $x = 6$ mm, τ_m is less than τ_G in all angles and the graphene will lay on top of the supporting board, as shown in Fig. 8(c). Figure 7(c) shows both the initial and final angles as y-axis for different distances x with $z = 4$ mm. In the gray region, no matter what the initial angle is, the final angle is always 0. In the white region, the final angle will move to the angle corresponding to the solid curve with the same x distance according to the black arrows. For example, in Fig. 7(c) with $z = 4$ mm and $x = 2$ mm, the initial angles of $\theta = 30°$ and $60°$ will lead to the same final tilted angle of

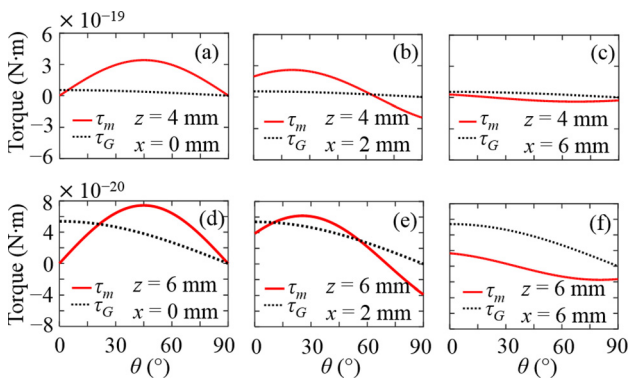

FIG. 8. Torque as a function of tilted angle at different x and z marked in the figure. τ_m and τ_G are the torques due to the magnetic field and gravity, respectively. We use τ_m in a direction that is opposite to the direction of τ_G so the balanced position occurs when $\tau_G = \tau_m$.

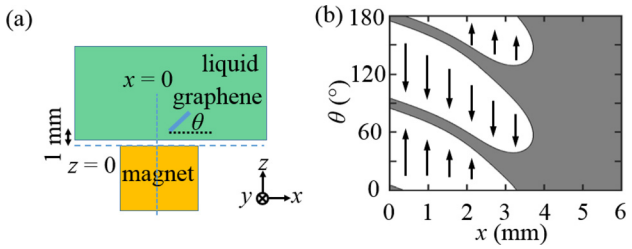

FIG. 9. (a) Schematic of the graphene flake in liquid. (b) Initial and final tilted angles when graphene flakes are located at different x distance in liquid. The graphene flake is located at 1 mm above the magnet. Gray region: the final angle is the same as the initial angle. White region: the final angle is moved until it reaches the edge of the gray region according to the direction indicated by the black arrows.

$\theta = 63°$. At a larger $z = 6$ mm as shown in Figs. 8(d)–8(f), there are always two intersect points between τ_m and τ_G curves until τ_m is always less than τ_G. The corresponding initial and final angles are plotted in Fig. 7(d). When $z = 2$ mm, the corresponding initial and final angles are similar to the case $z = 4$ mm, which are plotted in Fig. 7(b).

In a liquid environment, the graphene flake will float in the medium as a particle, as shown in Fig. 1(c). Figure 9(a) shows a schematic side view of graphene in liquid. The surrounding liquid has an effect of opposing the rotation of the particles. Different forces on graphene have been studied such as van der Waals force, electrostatic surface forces, gravity

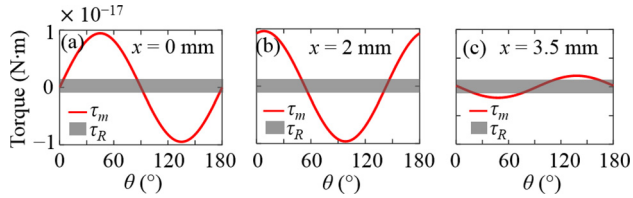

FIG. 10. Torque as a function of angle in liquid. Red solid curve: torque τ_m due to the magnetic force. Gray region: torque τ_R due to the resistance force.

force, buoyancy force, and Brownian movement force.[51–53] Previous studies show that these forces are much larger than gravity.[53] For simplicity, we consider the sum of the above mentioned forces as the total resistance force in the amount of 20 times gravity.[51–53] Figure 10 shows the τ_m induced by the magnetic field as a function of initial angle with different x distances. The gray region indicates the torque τ_R induced by the resistance force in liquid. When the value τ_m is inside the gray region, the resistance torque is larger than the magnetic torque and the graphene flake will not move. When the value τ_m is outside of the gray region, the graphene flake will move until the balanced angle is reached. Figure 9(b) shows both the initial and final angles as y-axis for different x. The gray region indicates that the flake will stay the same as the initial angle. In the white region, the torque due to the resistant force is less than the torque due to the magnetic force and the flake will rotate until the final angle reaches the edge of the gray

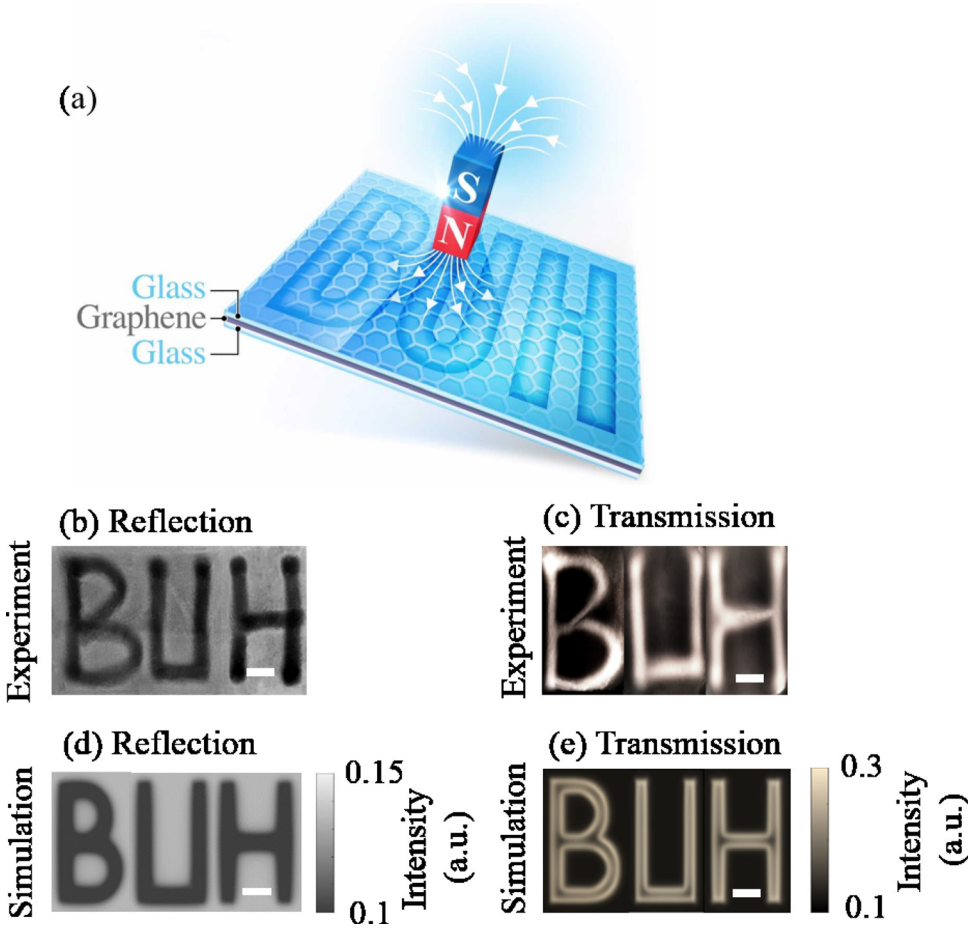

FIG. 11. (a) Schematic of a writing board. (b) and (c) Experimental reflection and transmission displays of "BUH" written by a bar magnet. (d) and (e) Simulations of reflection and transmission. The scale bars show a length of 10 mm.

region according to the direction indicated by the black arrows. We also study the results with a resistance force which is 15 or 25 times gravity in Fig. S4 (supplementary material) and the results do not significantly change.

A graphene magnetic writing board was recently proposed and developed.[22,54] This writing board uses graphene flakes with a strong orientation response to a magnetic field and orientation-dependent optical reflection and transmission. This paragraph explains simulations to model optical contrast on the writing board in the experiment. Figure 11(a) shows the schematic of the writing board with a permanent bar magnet. Graphene flakes were suspended in N-methyl-2-pyrrolidone (NMP) liquid with a thickness of 1 mm between two glass boards. Due to diamagnetism, the graphene flakes rotate according to the magnetic field when a bar magnet is placed on top of the writing board. When one observes the reflected light, dark lines could be created by sliding a pole of a bar magnet on top of the writing board. When the writing board is back illuminated, the dark lines appear bright. The reason is that the reflection and absorption are low, and transmission is high, when the graphene flake is vertically aligned.[22] Figures 11(b) and 11(c) show the letters written by a bar magnet in the reflection and transmission mode. We carried out simulation to determine the transmission and reflection using the finite-difference time-domain (FDTD) software from Lumerical. The procedure and analysis for the calculation of orientation-dependent transmission and reflection of one graphene flake can be found in the supporting information of Ref. 22. With the results of one graphene flake, we can further calculate the total transmission and reflection for 80 flakes floating in liquid, which is equivalent to a total graphene flake thickness of 400 nm in the light path. Based on the graphene flake angle at a particular distance with respect to the magnet as shown in Fig. 9, we can calculate total transmission and reflection at every position on the writing board. We assume totally randomized initial angles for all graphene flakes at every position inside the writing board. Figures 11(d) and 11(e) show the simulation results for the reflection and transmission of the letters "BUH" on the writing board. The computer simulations and experimental observations are in a very good agreement. Hence, the previous study and analysis from the Fig. 9 can be used to predict and model the optical contrast in devices using graphene flakes.

V. CONCLUSIONS

In summary, we show the balanced positions for graphite plates in a magnetic field due to the diamagnetic properties. We study torques in all three spatial directions in a non-uniform magnetic field. Millimeter-sized graphite plates in a regular polygon shape with an even number of sides can be levitated horizontally above four interleaved magnets. In addition, we also predict the final tilted angles of micrometer-sized graphene flakes in a magnetic field for both air and liquid environments. The diamagnetic force can be exploited to precisely control the orientation of graphene flakes. The ability to control the orientation of graphene flakes by magnetic fields allows for future research and development utilizing graphene flakes. Our study is expected to provide a useful tool to analyze and predict the macroscopic properties of graphene in future devices for electrical, thermal, and mechanical applications.

SUPPLEMENTARY MATERIAL

See supplementary material for additional information related to Figs. 2, 3, 6, and 9.

[1]K. S. Novoselov, A. K. Geim, S. V. Morozov, D. Jiang, Y. Zhang, S. V. Dubonos, I. V. Grigorieva, and A. A. Firsov, Science **306**, 666 (2004).
[2]X. Du, I. Skachko, A. Barker, and E. Y. Andrei, Nat. Nanotechnol. **3**, 491 (2008).
[3]C. Lee, X. Wei, J. W. Kysar, and J. Hone, Science **321**, 385 (2008).
[4]S. Stankovich, D. A. Dikin, G. H. B. Dommett, K. M. Kohlhaas, E. J. Zimney, E. A. Stach, R. D. Piner, S. T. Nguyen, and R. S. Ruoff, Nature **442**, 282 (2006).
[5]P. Chen and A. Alù, ACS Nano **5**, 5855 (2011).
[6]S. S. Gregersen, J. G. Pedersen, S. R. Power, and A. P. Jauho, Phys. Rev. B **91**, 115424 (2015).
[7]M. Liu, X. Yin, E. U. Avila, B. Geng, T. Zentgraf, L. Ju, F. Wang, and X. Zhang, Nature **474**, 64 (2011).
[8]M. Liu, X. Yin, and X. Zhang, Nano Lett. **12**, 1482 (2012).
[9]S. J. Koester and M. Li, Appl. Phys. Lett. **100**, 171107 (2012).
[10]W. Li, B. Chen, C. Meng, W. Fang, Y. Xiao, X. Li, Z. Hu, Y. Xu, L. Tong, H. Wang, W. Liu, J. Bao, and Y. R. Shen, Nano Lett. **14**, 955 (2014).
[11]J. S. Gmez-Daz and J. Perruisseau-Carrier, Opt. Express **21**, 15490 (2013).
[12]H. S. Chu and C. H. Gan, Appl. Phys. Lett. **102**, 231107 (2013).
[13]L. Wu, H. S. Chu, W. S. Koh, and E. P. Li, Opt. Express **18**, 14395 (2010).
[14]O. Salihoglu, S. Balci, and C. Kocabas, Appl. Phys. Lett. **100**, 213110 (2012).
[15]S. Zeng, K. V. Sreekanth, J. Shang, T. Yu, C. K. Chen, F. Yin, D. Baillargeat, P. Coquet, H. P. Ho, A. V. Kabashin, and K. T. Yong, Adv. Mater. **27**, 6163 (2015).
[16]W. Song, M. Cao, M. Lu, J. Yang, H. Ju, Z. Hou, J. Liu, J. Yuan, and L. Fan, Nanotechnology **24**, 115708 (2013).
[17]B. Tang, G. Hu, H. Gao, and L. Hai, Int. J. Heat Mass Transfer **85**, 420 (2015).
[18]H. Yan, Y. Tang, W. Long, and Y. Li, J. Mater. Sci. **49**, 5256 (2014).
[19]H. Babaei, P. Keblinski, and J. M. Khodadadi, Int. J. Heat Mass Transfer **58**, 209 (2013).
[20]H. Le Ferrand, S. Bolisetty, A. F. Demirrs, R. Libanori, A. R. Studart, and R. Mezzenga, Nat. Commun. **7**, 12078 (2016).
[21]B. Genorio, Z. W. Peng, W. Lu, B. K. P. Hoelscher, B. Novosel, and J. M. Tour, ACS Nano **6**, 10396 (2012).
[22]F. Lin, Z. Zhu, X. Zhou, W. Qiu, C. Niu, J. Hu, Y. Wang, Z. Zhao, D. Litvinov, Z. Liu, Z. M. Wang, and J. Bao, Adv. Mater. **29**, 1604453 (2017).
[23]Y. Ominato and M. Koshino, Phys. Rev. B **87**, 115433 (2013).
[24]Y. Ikezoe, N. Hirota, J. Nakagawa, and K. Kitazawa, Nature **393**, 749 (1998).
[25]A. K. Geim, M. D. Simon, M. I. Boamfa, and L. O. Heflinger, Nature **400**, 323 (1999).
[26]M. D. Simon, L. O. Heflinger, and A. K. Geim, Am. J. Phys. **69**, 702 (2001).
[27]J. W. McClure, Phys. Rev. **104**, 666 (1956).
[28]J. Nguyen, S. Contera, and I. L. Garcia, RSC Adv. **6**, 46643 (2016).
[29]L. He, J. Ye, M. Shuai, Z. Zhu, X. Zhou, Y. Wang, Y. Li, Z. Su, H. Zhang, Y. Chen, Z. Liu, Z. Cheng, and J. Bao, Nanoscale **7**, 1616 (2015).
[30]Q. Li, K. S. Kim, and A. Rydberg, Rev. Sci. Instrum. **77**, 065105 (2006).
[31]M. Kobayashi and J. Abe, J. Am. Chem. Soc. **134**, 20593 (2012).
[32]C. M. Olmos, H. I. Rassol, B. H. Weiller, and J. K. Gimzewski, ACS Nano **7**, 4164 (2013).
[33]X. Zang, Q. Zhou, J. Chang, Y. Liu, and L. Lin, Microelectron. Eng. **132**, 192 (2015).
[34]P. X.-L. Feng, Nat. Nanotechnol. **8**, 897 (2013).
[35]T. Hallam, C. F. Moldovan, K. Gajewski, A. M. Lonescu, and G. S. Duesbberg, Phys. Status Solidi B **252**, 2429 (2015).
[36]P. Vavassori, M. Pancaldi, M. J. Perez-Roldan, A. Chuvilin, and A. Berger, Small **12**, 1013 (2016).

[37]R. D. Waldron, Rev. Sci. Instrum. **37**, 29 (1966).
[38]H. B. Profijt, C. Pigot, G. Reyne, R. M. Grechishkin, and O. Cugat, J. Magn. Magn. Mater. **321**, 259 (2009).
[39]G. D. Pasquale, S. Iamoni, and A. Somà, Int. J. Mech. Sci. **68**, 56 (2013).
[40]G. Kstler, I. V. Nemoianu, and E. Cazacu, IEEE Trans. Magn. **48**, 4793 (2012).
[41]E. P. Furlani, *Permanent Magnet and Electromechanical Devices: Materials, Analysis and Applications* (Academic Press, 2001).
[42]N. Derby and S. Olbert, Am. J. Phys. **78**, 229 (2010).
[43]J. T. Conway, IEEE Trans. Magn. **37**, 2977 (2001).
[44]B. vanNinhuijs, T. E. Motoasca, B. L. J. Gysen, and E. A. Lomonova, IEEE Trans. Magn. **49**, 4109 (2013).
[45]J. L. G. Janssen, J. J. H. Paulides, and E. A. Lomonova, IEEE Trans. Magn. **45**, 4628 (2009).
[46]C. S. Siyambalapitiya, *Model and Validation of Static and Dynamic Behavior of Passive Diamagnetic Levitation for Energy Harvesting* (University of South Florida, ProQuest Dissertations Publishing, 2012).
[47]M. Kustov, *Characterization and Design of Micro-Magnets for the Diamagnetic Levitation of Micro-and Nanoparticles* (Universite de Grenoble, 2010).
[48]T. B. Jones, *Electromechanics of Particles* (Cambridge University Press, Cambridge, 1995).
[49]R. K. Arora, IEEE Trans. Magn. **25**, 2789 (1989).
[50]N. Tabat, H. S. Edelman, D. Song, and T. Vogt, Appl. Phys. Lett. **106**, 092405 (2015).
[51]B. J. Robinson and O. V. Kolosov, Nanoscale **6**, 10806 (2014).
[52]J. Britton, N. E. A. Cousens, S. W. Coles, C. D. van Engers, V. Babenko, A. T. Murdock, A. Kos, S. Perkin, and N. Grobert, Langmuir **30**, 11485 (2014).
[53]H. P. Zhu, Z. Y. Zhou, R. Y. Yang, and A. B. Yu, Chem. Eng. Sci. **62**, 3378 (2007).
[54]C. Niu, F. Lin, Z. Zhu, X. Zhou, Z. Liu, Z. Wang, J. Bao, and J. Hu, in *OSA Technical Digest - Conference on Lasers and Eletro-Optics* (Optical Society of America, 2017), paper SW4K.5.